

## Critical-point phonon frequencies of diamond

Claude A. Klein, Thomas M. Hartnett, and Clifford J. Robinson  
*Raytheon Company, Research Division, Lexington, Massachusetts 02173*

(Received 21 October 1991)

The phonon-dispersion curves derived from neutron-scattering experiments performed on diamond [J. Warren *et al.*, Phys. Rev. **158**, 805 (1967)] are not accurate enough to yield the exact frequencies of critical-point (CP) phonons and, thus, to provide a satisfactory interpretation of second-order optical spectra. A self-consistent analysis of such spectra [S. Solin and A. Ramdas, Phys. Rev. B **1**, 1687 (1970)] was not fully successful because of ambiguities that arise in assigning second-order infrared absorptions and features in the Raman spectra to specific two-phonon summations. A more effective method for obtaining accurate CP phonon frequencies involves investigating defect-activated one-phonon absorptions; in this paper, we take advantage of the availability of chemically vapor-deposited (CVD) diamond for the purpose of locating and assigning infrared (ir) absorption features in the one-phonon region to CP phonons at the Brillouin-zone boundary. Fourier-transform ir absorbance spectra of CVD diamond exhibit a complex structure at wave numbers below the  $1332.5\text{-cm}^{-1}$  lattice-mode cutoff, which is induced by impurity-associated defect centers and yields the exact positions of 16 zone-edge CP phonons. In conjunction with the triply degenerate zone-center mode, this set of phonons then provides the basis for predicting the positions of second-order optical features through simple summations. When the selection rules are taken into account, the procedure yields excellent results, not only in terms of CVD-diamond ir spectra, but also in regard to earlier measurements of the intrinsic two-phonon absorption coefficient of type-IIa natural diamond [J. Hardy and S. Smith, Philos. Mag. **6**, 1163 (1961)] and the second-order polarization-dependent Raman spectra recorded by Solin and Ramdas.

### I. INTRODUCTION

Recent, major advances in the art of growing diamond by low-pressure chemical vapor-deposition (CVD) techniques<sup>1</sup> has stimulated enormous interest, since the properties of these deposits appear to match those of natural diamond crystals. At this time, much of the interest concerns potential applications involving infrared (ir) transmitting windows for adverse environments,<sup>2</sup> which requires a thorough characterization of this material's optical properties. Infrared absorption in diamond occurs as a result of processes that generate optical and acoustical phonons, thus reflecting lattice vibrational characteristics.<sup>3</sup> These characteristics are best described in the light of phonon-dispersion relations. For diamond, a complete set of dispersion curves has been available for some time, based on coherent inelastic neutron-scattering experiments performed by Warren *et al.*;<sup>4</sup> these dispersions represent intrinsic characteristics of the diamond lattice and are little affected by the presence of even large impurity concentrations. They are, however, not accurate enough to yield the exact frequencies of critical-point (CP) phonons and, thus, to provide a satisfactory interpretation of the second-order ir absorption features of diamond as recorded by Hardy and Smith<sup>5</sup> in 1961. Much progress was made, ten years later, when Solin and Ramdas<sup>6</sup> carried out a detailed investigation of the first- and second-order Raman scattering in diamond, taking polarization effects into account. The complex structure exhibited by second-order Raman spectra in various geometries was interpreted in terms of summations of CP

phonons that obey relevant symmetry criteria, and was shown to be consistent with available infrared-absorption<sup>5</sup> and neutron-scattering<sup>4</sup> data. There remain, however, some prominent infrared and Raman features that do not fit the Solin-Ramdas scheme, thus creating an issue, especially in the context of a theoretical paradigm that enforces all applicable selection rules.

Much of the problem<sup>7</sup> arises because it is not a straightforward task to assign second-order features to specific two-phonon summations, considering the multiplicity of phonon branches, and the fact that neutron-scattering data do not match the accuracy of optical spectroscopy. In this regard, it is important to bear in mind that, although the direct absorption of incident photons by single phonons cannot take place in an ideal diamond-type crystal,<sup>8</sup> it may occur in the presence of defects that disrupt the periodicity of the lattice. Defect-induced one-phonon absorption thus provides a direct method for observing lattice vibrational effects and has proven quite effective for investigating intrinsic phonon-frequency spectra as well as the nature of inserted impurities or imperfections.<sup>3</sup> In fact, as early as 1960, band-mode single-phonon absorption has been observed in neutron-irradiated type-IIa diamond,<sup>9</sup> which led to an attempt to identify "characteristic" phonons in this material. Since the CVD diamonds of current interest are polycrystalline and defect rich,<sup>1</sup> it should not be surprising that we may take advantage of this situation for the purpose of locating and assigning spectral features in the one-phonon region to CP phonons in the Brillouin zone (BZ). Furthermore, the advent of convenient instrumentation to perform Fourier-transform infrared spectroscopy

py (FTIR) provides us with vastly improved spectra in terms of resolution and reproducibility, which should allow us to interpret the features on much sounder basis; in this connection, we may emphasize that the one-phonon absorption region of diamond encompasses the 8–12- $\mu\text{m}$  spectral range, thus covering a wavelength “window” of major importance in contemporary ir technology.

The purpose of the present paper is as follows. First, we shall report on single-phonon absorptions in a more elaborate manner than earlier<sup>10</sup> and present a corrected table of CP phonon frequencies in diamond, which takes into account additional measurements and reflects considerations relating to the slope of the dispersion at the zone edge. This set of CP phonons then provides the basis for “predicting” the positions of second-order features through simple summations (overtones and combinations) that obey the relevant selection rules; the procedure yields excellent results not only for two-phonon ir absorptions but also in the context of interpreting second-order Raman shifts. For the convenience of the reader, we will begin by briefly reviewing relevant aspects of the lattice dynamics of diamond and discussing the fundamentals of defect-activated one-phonon absorption mechanisms (Sec. II). In Sec. III, we describe our diamond specimens and comment on the experimental procedure that allows us to enhance the spectral features and to generate detailed absorption traces for obtaining meaningful indications about lattice-mode phonons as well as residual impurities. The data are presented in Secs. IV and V; there was no attempt made to assess the temperature dependence because it is not likely that information of this nature can shed more light on phonon assignments. Specifically, Sec. IV deals with defect-activated one-phonon absorption as in Ref. 10 but focuses on CP phonons, since it is now our objective to obtain a complete listing of CP phonon frequencies suitable for “fitting” the two-phonon spectra. As will be demonstrated in Sec. V, this has been achieved not only in terms of our own measurements but also with regard to earlier measurements of the intrinsic ir absorption coefficient of natural diamond<sup>5</sup> and the second-order Raman characteristics described by Solin and Ramdas.<sup>6</sup> The conclusions are stated in Sec. VI.

## II. THEORETICAL CONSIDERATIONS

In the infrared, the optical properties of a perfect diamond crystal reflect the density of vibrational modes,<sup>11</sup> which in turn derives from phonon-dispersion curves as illustrated in Fig. 1. These dispersions refer to the main symmetry directions in the Brillouin zone, i.e.,

$$\Delta [\mathbf{q}=2\pi(\zeta, 0, 0)/a], \quad (1a)$$

$$\Sigma [\mathbf{q}=2\pi(\zeta, \zeta, 0)/a], \quad (1b)$$

$$\Lambda [\mathbf{q}=2\pi(\zeta, \zeta, \zeta)/a], \quad (1c)$$

where  $\mathbf{q}$  represents the phonon wave vector,  $\zeta$  designates a BZ coordinate, and  $a$  is the lattice constant. They are displayed here<sup>12</sup> as generated by a Born–von Kármán model fit<sup>13</sup> to the neutron-scattering data of Warren *et al.*<sup>4</sup> Regarding these measurements, it is important to

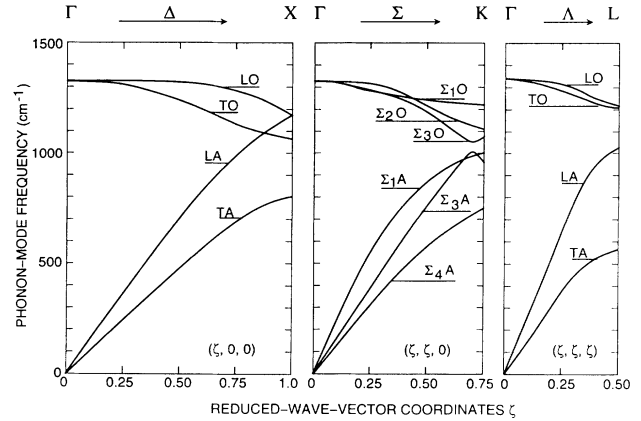


FIG. 1. Phonon-dispersion curves of diamond, along the main symmetry directions.

keep in mind that neutron spectroscopy does not yield precise numbers for the phonon frequencies; the dispersions plotted in Fig. 1 may have errors of at least 3%, which says that much remains to be done to accurately describe the lattice dynamics of diamond. In principle, the two atoms per primitive cell give rise to six vibrational frequencies for each propagation vector, which leads to three acoustical and three optical branches in the phonon-dispersion picture; as evidenced in Fig. 1, degeneracies do occur, at the center of the zone (point  $\Gamma$ ) in particular, which supports a triply degenerate optical mode of  $\Gamma^{(25^+)}$  symmetry that is Raman active in the first order. Since the distribution of vibrational modes is dominated by short-wavelength phonons near the zone boundary,<sup>3</sup> there will be singularities (see, for instance, the density of modes obtained by Tubino, Piseri, and Zerbi<sup>14</sup> and reproduced in Fig. 4) that originate at critical points in the Brillouin zone. On the basis of topological considerations alone, diamondlike crystals have four zone-edge CP's,

$$\mathbf{q}_X = (2\pi/a)(1, 0, 0), \quad \mathbf{q}_L = (2\pi/a)(1/2, 1/2, 1/2), \quad (2a)$$

$$\mathbf{q}_K = (2\pi/a)(3/4, 3/4, 0), \quad \mathbf{q}_W = (2\pi/a)(1, 1/2, 0), \quad (2b)$$

but additional (“accidental”) critical points may emerge depending upon the actual force field, or in other words, the shape of the dispersions within the Brillouin zone.

In perfect diamond, there is only one optically active mode: The zone-center triply degenerate mode that is Raman active but is forbidden. It gives rise to a Raman shift of  $1332 \pm 0.5 \text{ cm}^{-1}$ ,<sup>6</sup> which fits the dispersion curves derived from neutron-scattering experiments (see Fig. 1), and represents the highest-frequency vibrational mode propagating through the lattice. Since this vibration does not induce any change in the dipole moment, ideal diamond lattices are therefore transparent in the first order. In the presence of “defects,” however, some absorption can occur because impurities, imperfections, or disorder destroy the translational symmetry, which causes a

breakdown of the momentum-conservation law and allows lattice modes to couple with electromagnetic radiation; optical spectroscopy of defect-rich diamond may thus provide information on phonons that possess finite wave vectors. In this context, it is essential to distinguish the case of (a) *localized-mode phonons* associated with low-atomic-number, relatively strongly bound defects whose resonance frequency exceeds that of the Raman phonon thus prohibiting propagation, and (b) *lattice-mode phonons* activated by “heavy” and/or weakly bound impurities that include resonance-excited modes as well as intrinsic vibrational modes. In this lattice or band-mode regime, the absorption coefficient can be expressed<sup>15</sup> in the following manner:

$$\beta(\omega) = \frac{\pi D e^2}{3 n c \epsilon_0} |X(\omega)|^2 S(\omega), \quad (3)$$

if  $D$  refers to the defect concentration,  $X(\omega)$  represents the frequency-dependent defect-induced dipole moment, and  $S(\omega)$  describes the density of states of the host lattice. The absorption thus maps the vibrational mode density, provided that the coupling coefficient  $X(\omega)$  is a weak function of frequency in the spectral range of interest;<sup>16</sup> and, since singularities in the density of modes originate from phonons located at critical points in the Brillouin zone, it follows that the features exhibited by defect-activated first-order absorption spectra may throw light on CP phonons in a very direct manner.

Higher-order processes occur when two or more phonons simultaneously interact with incident phonons to produce infrared absorption or Raman scattering. With diamondlike crystals, a dipole cannot be created by mechanical anharmonicity, but the simultaneous “emission” of two phonons of opposite momentum may result in a second-order electrical dipole moment with which electromagnetic radiation can couple. If relevant selection rules are satisfied, absorption takes place when the frequency of the exciting radiation equals the sum of the frequencies of the two active phonons, which implies it must be proportional to the combined density of modes. Hence, if the coupling matrix element is a weak function of frequency, the combined density of modes controls the shape of the absorption spectrum; and, since the singularities of the combined density give rise to features in the two-phonon region, it is clear that Brillouin-zone critical-points again play a pivotal role.<sup>17</sup> Similar considerations apply to the second-order Raman spectrum in the sense that structure reflects the joint density of states if the scattering cross section is a smooth function of the frequency shift. In principle, critical points manifest themselves only if the process is consistent with the selection rules for dipole or Raman activity; these rules derive from group-theoretical arguments<sup>18</sup> and concern phonon combinations as well as overtones.

### III. EXPERIMENTAL CONSIDERATIONS

The CVD-diamond specimens that we report on in this paper were grown on polished molybdenum and polished silicon substrates by means of either microwave-plasma or hot-filament assisted reduced-pressure depositions

from dilute-methane–hydrogen mixtures at temperatures of about 900 °C. These deposits are 200–400  $\mu\text{m}$  thick; they are clear and colorless in the visible but show faceted growth surfaces indicative of polycrystalline aggregates with grain sizes of the order of 10  $\mu\text{m}$ . The hydrogen content, as determined by secondary ion mass spectroscopy, is believed to be below the 0.01 at. % level, which points to outstanding crystalline quality. First-order Raman spectra as in Fig. 2 display a sharp intense line at 1332.5  $\text{cm}^{-1}$ , in accord with measurements that were carried out on single crystals,<sup>6</sup> and show no evidence of Raman shifts in the 1350- $\text{cm}^{-1}$  wave-number range and, thus, no evidence of  $\text{sp}^2$ -bonded carbon.<sup>19</sup> The full width at half maximum (FWHM), which is known to provide a good measure of the crystalline quality, varies with the deposition conditions and the local morphology but tends to be in the 3–4- $\text{cm}^{-1}$  range; such widths are not quite comparable to those of gem-quality diamonds (FWHM  $\approx 2 \text{ cm}^{-1}$  at room temperature), thus reflecting the presence of some lattice disorder. In this context, we may consider the mechanism that determines the width of the first-order Raman line:<sup>20</sup> Since the degenerate zone-center optical phonon decays into two acoustic modes of equal and opposite wave vector, the broadening arises from the reduced optical-phonon lifetime caused by scattering from lattice defects and/or inhomogeneous stresses. The recently investigated effects of isotopic disorder on both frequency and width of the Raman line<sup>21</sup> may also be of relevance in this context.

In Fig. 3, we display the ir-transmittance trace of a partly polished microwave-plasma CVD-diamond specimen and compare it to the transmittance of a type-IIa diamond with good surfaces. The two traces refer to the specular transmittance at near-normal incidence and are as recorded on an FTIR Bomem Inc. spectrometer (model MB-120) operating at a resolution of 4  $\text{cm}^{-1}$ , the instrument control computer collecting and co-adding one hundred scans per run. Three comments are in order.

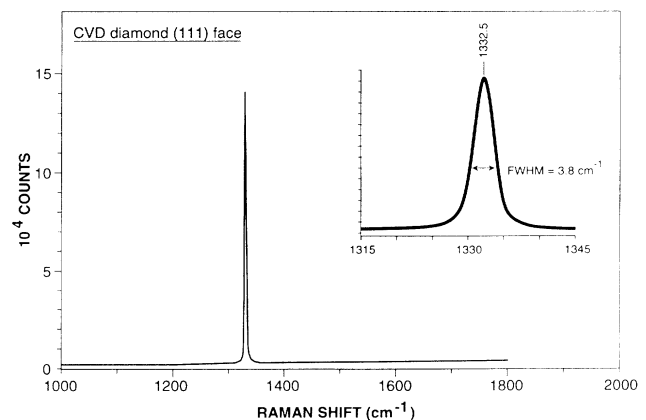


FIG. 2. First-order Raman spectrum of a chemically vapor-deposited diamond specimen obtained by means of the microwave-plasma assisted process. The spectrum was acquired on a J-Y Optical Systems instrument (model U-1000) using the 514.5-nm argon-ion laser line and taking data points every 0.25  $\text{cm}^{-1}$  in the critical 1315–1345  $\text{cm}^{-1}$  frequency range.

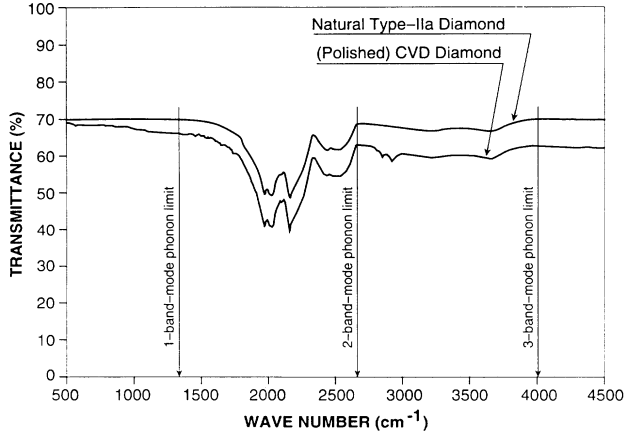


FIG. 3. Compares the measured infrared transmittance of a partially polished chemically vapor-deposited diamond with that of a type-IIa natural specimen. The two diamonds are of similar thickness. The highest-frequency band-mode phonon is at  $1332.5 \text{ cm}^{-1}$  (Raman phonon).

(i) The loss in transmittance experienced by the CVD specimen must be attributed to nonspecular reflections caused by surface roughness. These losses, which are proportional to  $(\sigma n / \lambda)^2$ , tend to increase at higher wave numbers, as the wavelength of the incident light becomes comparable to the facets' dimensions, i.e., the roughness scale  $\sigma$ . In the  $20\text{-}\mu\text{m}$  wavelength range ( $\nu \approx 500 \text{ cm}^{-1}$ ), the "scatter" appears to be minimal (see Fig. 3), in the sense that the transmittance almost matches that of natural diamond ( $T \approx 70\%$ ), which in turn almost agrees with the predicted absorption-free transmittance,

$$T_0 = \frac{1-R}{1+R} = \frac{2n}{1+n^2}, \quad (4)$$

on setting the refractive index  $n$  equal to 2.38, as inferred from a Herzberger-type dispersion formula,<sup>22</sup> at  $20 \mu\text{m}$ .

(ii) Since the Raman phonon of diamond ( $\nu = 1332.5 \text{ cm}^{-1}$ ) represents the band-mode phonon that has the highest energy (see Fig. 1), it follows that the  $500\text{--}4500\text{-cm}^{-1}$  wave-number range covered in Fig. 3 encompasses the one-, two-, and three-phonon absorption regimes, thus providing an overview of lattice dynamical effects in this material. Evidently, the dominant absorption occurs in the two-phonon region, which exhibits an abrupt cutoff at exactly  $2O(\Gamma) = 2665 \text{ cm}^{-1}$  and is not affected by lattice defects, in accord with previous observations for CVD diamond.<sup>23</sup> For both, chemically vapor-deposited and natural single crystals, there are some weak, more diffuse bands in the three-phonon region, but beyond  $4000$  wave numbers ( $\lambda < 2.5 \mu\text{m}$ ), there is no detectable absorption.

(iii) The absorption-band doublet at  $2854\text{--}2923 \text{ cm}^{-1}$ , which is not seen in natural diamond, has attracted much attention because its strength appears to be linked to the methane pressure in the deposition chamber;<sup>23</sup> this doublet has been attributed to  $CH_x$  "stretch" modes and is

believed to reflect the residual hydrogen content. Furthermore, there is evidence to suggest that localized modes ( $\nu > 1333 \text{ cm}^{-1}$ ) as observed in CVD diamond (see Fig. 3) always emerge in conjunction with the  $CH_x$  doublet, which points to hydrogen as the responsible impurity. The lattice-mode phonons ( $\nu < 1333 \text{ cm}^{-1}$ ), however, must involve additional substitutional impurities or defect aggregates that we have identified as nitrogen related, in a previous paper.<sup>10</sup> In that context, we made use of a procedure<sup>24</sup> that amounts to evaluating apparent absorbances defined as

$$A^* = \ln(T_0^*/T), \quad (5)$$

where  $T$  is the measured transmittance and  $T_0^*$  refers to an *ad hoc* "baseline fit." This fit (in effect, a polynomial approximation) serves the purpose of eliminating weakly frequency-dependent transmittance losses originating from surface effects and, thus, to enhance bulk-

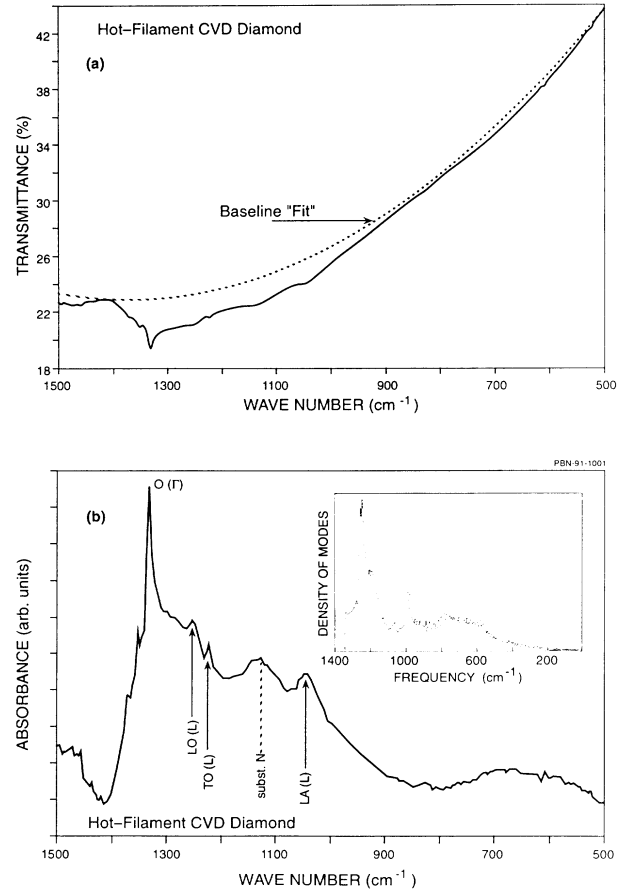


FIG. 4. Spectral transmittance (a) and apparent absorbance (b) of a chemically vapor-deposited diamond specimen grown at The Pennsylvania State University. The baseline was obtained by means of a parabolic fit that assumes zero absorption at the onset of the two-phonon summations ( $\nu \approx 1400 \text{ cm}^{-1}$ ) and for phonon modes in the low-frequency acoustic range ( $\nu \lesssim 500 \text{ cm}^{-1}$ ). On using the baseline fit as a reference transmittance, the absorbance is seen to map the density of modes of perfect diamond obtained in Ref. 14.

absorption-related strongly frequency-dependent spectral features. Figure 4 demonstrates how the procedure works with a lower-quality CVD-diamond specimen. This specimen exhibits poor transmittance in the 10- $\mu\text{m}$  region, owing to its surface roughness, but the “subtraction of the background” by means of Eq. (5) yields an apparent absorbance with well-resolved features that are easily amenable to interpretation [see Fig. 4(b)].<sup>25</sup> In this connection, we emphasize that an apparent absorbance as defined in Eq. (5) should not be utilized to extract absorption coefficients. Or more precisely, one should not write

$$\beta = \frac{\ln(T_0^*/T)}{t}, \quad (6)$$

where  $t$  is the thickness, unless the two following conditions are met: (a) The baseline fit images the true transmittance in the absence of absorption losses, and (b) the measured absorbance is much smaller than unity.

#### IV. ONE-PHONON FEATURES

The absorbance traces reproduced in Figs. 5 and 6 demonstrate that the above outlined subtraction procedure yields a surprisingly rich structure at wave numbers below 1400  $\text{cm}^{-1}$ , which can be interpreted in the light of available information on intrinsic vibrational modes of diamond<sup>4</sup> and on ir resonance bands associated with substitutional impurities and/or defect centers.<sup>26</sup> The CP assignments were first made on the basis of comparing the positions of intense and clearly reproducible features with the zone-edge phonon frequencies obtained through inelastic neutron scattering; because of the large uncertainties affecting the measurements,<sup>27</sup> some of these assignments are rather ambiguous, but more reliable identifications can be made by ensuring that the stronger peaks reflect zero-gradient phonon dispersions at the

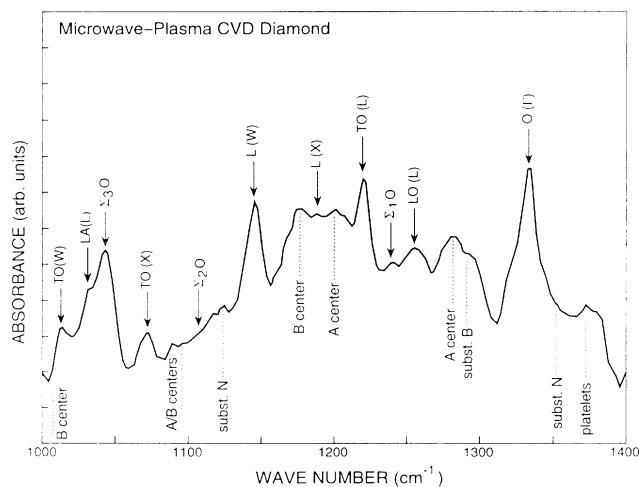


FIG. 5. Apparent absorbance of a state-of-the-art chemically vapor-deposited diamond, in the one-optical-phonon spectral region. Critical-point phonon absorption lines are identified by downward pointing arrows. Impurity-related resonance absorptions are as specified in Ref. 10.

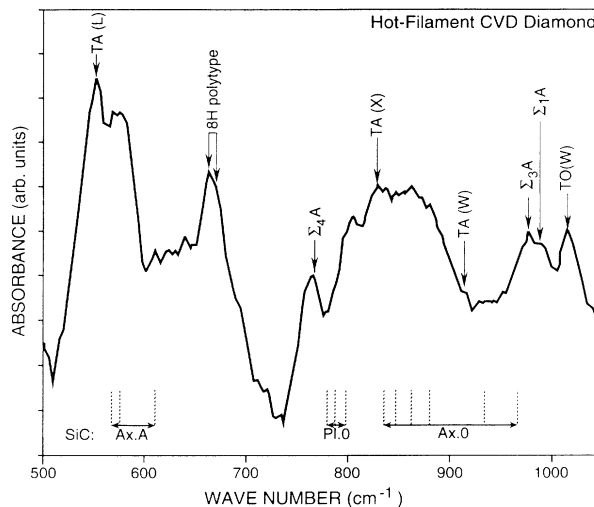


FIG. 6. Apparent absorbance of an “older” chemically vapor-deposited diamond, in the one-acoustic-phonon spectral region. Critical-point phonon absorption lines are identified by downward pointing arrows. The silicon carbide lines originate from axial-acoustic, planar-optical, and axial-optical modes as described in Ref. 29.

zone edge. We believe that, in this manner, we have been able to not only detect the 16 topological CP’s at symmetry points  $X$ ,  $L$ ,  $K$ , and  $W$ , but also to make assignments that should be correct.

Figure 5 refers to a CVD-diamond specimen of superior quality, based on hydrogen content, and depicts the spectral absorption features in the 1000–1400- $\text{cm}^{-1}$  wave-number range. Perhaps most striking is the prominent line at 1333  $\text{cm}^{-1}$ , which obviously derives from the zone-center Raman phonon and, thus, points to di-

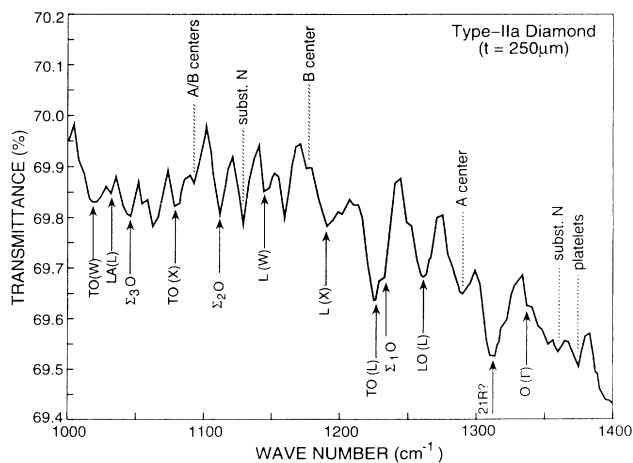


FIG. 7. Measured transmittance of a type-IIa natural diamond, in the one-phonon regime. Critical-point phonon absorption lines are identified by upward pointing arrows. Impurity-related resonance absorptions are as specified in Ref. 10.

pole activity induced by residual defects; in addition, the nine optical zone-edge CP's are clearly in evidence, with the exception of the  $\Sigma_2$ O phonon at point  $K$  that can be seen in Fig. 7. With regard to crystal imperfections, Fig. 5 exhibits an interesting pattern in the sense that all the classic<sup>26</sup> nitrogen-related "species" have been detected (see Ref. 10 for a discussion), which correlates well with cathodoluminescence-based observations<sup>28</sup> and made it possible to identify virtually all the features displayed in Fig. 5.

At wave numbers of less than  $1000 \text{ cm}^{-1}$ , the situation proved less favorable, which made it difficult to obtain precise numbers for the frequencies of relevant CP phonons. There are two reasons for this: (a) The response of our FTIR instrument degrades owing to enhanced noise at longer wavelengths, and (b) the signals now originate from acoustic phonons of relatively low density of states (see Fig. 4). Our best spectrum is the one reproduced in Fig. 6, which refers to hot-filament-grown material deposited on silicon and, unfortunately, exhibits features<sup>29</sup> that originate from a nondiamond phase (SiC polytypes) that masks, to some extent, the transverse-acoustic diamond modes of interest.

The critical-point phonon frequencies derived from an examination of the apparent absorbance of CVD diamond in the single-phonon regime are listed in Table I (fifth column) with estimated uncertainties that reflect repeated observations on a variety of specimens, including near-single-crystal deposits.<sup>30</sup> These frequencies are much more accurate than those deduced by means of neutron spectroscopy (third column) but always fall

within the error brackets of the Los Alamos assignments.<sup>4</sup> Also listed are the Solin-Ramdass assignments,<sup>6</sup> which derive from an analysis of the two-phonon Raman scatter in diamond, taking earlier<sup>5</sup> two-phonon ir absorption data into account; a comparison of the fourth and fifth columns reveals some serious discrepancies that require further attention (see Sec. V). But first, it should be of interest to evaluate Brout's sum,  $\sum_i \omega_i^2(\mathbf{q})$ , at all the BZ points for which we now have what appears to be accurate phonon energies: The sum involves the six branches of the phonon dispersion, including the degeneracies, and yields numbers as recorded in Table I (sixth column), at the key symmetry points. Evidently, the sum is not the same at the center and the edge of the zone, thus confirming that the sum rule does not apply to diamond;<sup>31</sup> in fact, we have

$$\sum_{i=1}^6 \omega_i^2(\mathbf{q}) > \sum_{i=1}^6 \omega_i^2(\mathbf{0}) \quad (7)$$

at the BZ edge, which is indicative of nonelectrostatic interatomic forces in this material. Still, we find that Brout's equation as modified by Mitra and Marshall,<sup>32</sup>

$$\sum_{i=1}^6 \omega_i^2(\mathbf{q}) = 16\sqrt{3}r_0/(\chi\mu), \quad (8)$$

yields  $1.91 \times 10^{29} \text{ Hz}^2$  upon inserting proper numbers<sup>33</sup> for the internuclear distance  $r_0$ , the bulk compressibility  $\chi$ , and the reduced mass  $\mu$ ; this result agrees quite well with the measured sum at point  $\Gamma$ ,

TABLE I. Critical-point phonon frequencies (in  $\text{cm}^{-1}$ ) of diamond.

Symmetry point	Phonon branch <sup>a</sup>	"Neutron" Ref. 4	"Optical" Ref. 6	This work	Brout sum ( $10^{29} \text{ Hz}^2$ )
$\Gamma$	$\Delta_2'(O), \Delta_5(O)$		1332.5±0.5	1332.5±1	1.89
$X$	$\Delta_2'(O), \Delta_1(A)$	1184±21	1185±5	1191±3	2.31
	$\Delta_5(O)$	1072±26	1069±5	1072±2	
	$\Delta_5(A)$	807±32	807±5	829±2	
$L$	$\Lambda_1(O)$	1242±37	1252±5	1256±4	2.21
	$\Lambda_3(O)$	1210±37	1206±5	1220±2	
	$\Lambda_1(A)$	1035±32	1006±5	1033±2	
	$\Lambda_3(A)$	552±16	563±5	553±2	
$K$	$\Sigma_1(O)$	1232±27 <sup>b</sup>	1230±5	1239±2	2.26
	$\Sigma_2(O)$	1110±21 <sup>b</sup>	1109±5	1111±1	
	$\Sigma_3(O)$	1046±21	1045±5	1042±2	
	$\Sigma_1(A)$	1009±16 <sup>b</sup>	988±5	992±3	
	$\Sigma_3(A)$	972±16	980±5	978±1	
	$\Sigma_4(A)$	765±21 <sup>b</sup>	· · ·	764±4	
$W$	$Z(U)$		1179±5	1146±1	2.27
	$Z(M)$	993±53	999±5	1019±3	
	$Z(L)$	919±11	908±5	918±12 <sup>c</sup>	

<sup>a</sup>The notations are as in Ref. 4.

<sup>b</sup>Interpolated using Newton's method.

<sup>c</sup>Very weak feature and not always discernible.

$$\sum_{i=1}^6 \omega_i^2(0) = 1.89 \times 10^{29} \text{ Hz}^2, \quad (9)$$

and, therefore, has important theoretical implications. For the sake of completeness, we are also including here (see Fig. 7) the 1000–1400-cm<sup>-1</sup> wave-number segment of the FTIR-measured transmittance of a purchased single-crystal type-IIa diamond. The previously identified single-phonon features are clearly apparent,<sup>34</sup> thus suggesting that the Lax-Burstein prescription<sup>8</sup> does not apply, even in high-purity natural diamond; similar observations were recently made by Thomas and Joseph,<sup>35</sup> who detected four lattice-mode absorption lines in type-IIa diamond. Evidently (see Fig. 7), these are nitrogen-induced one-phonon bands, which brings back to mind an old contention of Davies<sup>26</sup> that “the type-IIa classification is thus doomed to obsolescence as soon as a higher sensitivity (method) of detecting *A* and *B* nitrogen aggregates becomes available.”

V. TWO-PHONON FEATURES

To be considered successful, the task of obtaining CP phonon frequencies from defect-activated single-mode absorptions must yield a set of phonons that can explain most if not all the features exhibited by second-order optical spectra. Furthermore, this must be done (see Sec. II) on the basis of simple summations,<sup>36</sup> i.e.,

$$\hbar\omega = \hbar(\omega_1 + \omega_2), \quad (10)$$

if  $\omega$  is the frequency of the observed feature, and  $\omega_1, \omega_2$  are the two CP phonons involved, keeping in mind that Eq. (10) refers to combinations ( $\omega_1 \neq \omega_2$ ) as well as overtones ( $\omega_1 = \omega_2$ ), depending upon applicable selection rules.<sup>18</sup> In this section, we will assess in some detail how well the CP phonon listed in Table I “fit” the two-phonon absorption spectra but confine our analysis of the two-phonon Raman process to a single configuration because an exhaustive, unambiguous investigation far exceeds the scope of the present paper.

Figure 8 displays the entire two-phonon ir absorption spectrum of diamond, as obtained for “good” CVD material, and demonstrates that, indeed, most of the significant features can be interpreted in terms of the 17 phonons listed in the fifth column of Table I. (a) The lowest-frequency ir-active combination ( $\Sigma_3A + \Sigma_4A$ ) emerges at 1742 cm<sup>-1</sup> and sets the stage for stronger absorptions such as the LO(*L*)+TA(*L*) summation, which involve optic branches. The very weak, quasicontinuous features in the 1400–1600-cm<sup>-1</sup> range must be ascribed to localized modes, mainly associated with hydrogen in various bonding configurations. (b) The three characteristic, rather intense bands in the 1900–2200-wave-number range provide a sensitive means of verifying the accuracy of our assignments and will be examined later on. (c) The broad minimum at approximately 2330 cm<sup>-1</sup> does not correlate well with predictions, since the closest forbidden summations yield

$$2L(W) < 2330\text{cm}^{-1} < \Sigma_1O + \Sigma_2O. \quad (11)$$

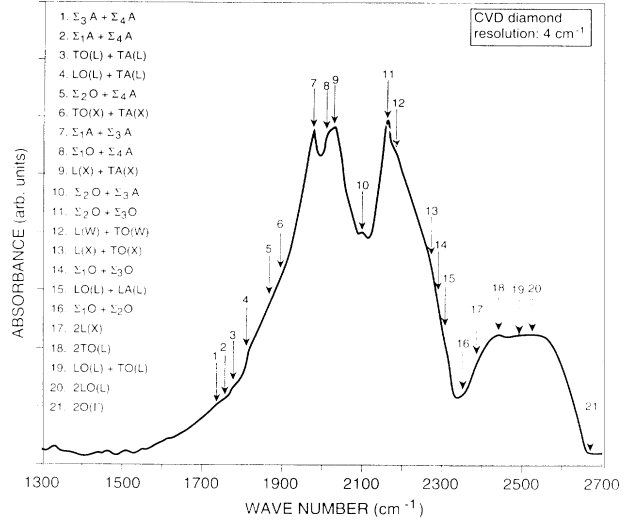


FIG. 8. Absorbance spectrum of a state-of-the-art chemically vapor-deposited diamond, in the two-phonon regime. Critical-point phonon assignments are in accord with column 5 of Table I. Dashed arrows refer to intrinsically dipole-inactive summations.

Beyond that point, there are no dipole-active summations, which leads us to conclude that the diffuse absorption exhibited by diamond crystals at the tail end of the two-phonon region reflects a relaxation of the selection rules, in particular with regard to phonons belonging to the same branch.

In principle, there are 19 CP phonon summations that fall between 1937 cm<sup>-1</sup> (TO+TA at point *W*) and 2253 cm<sup>-1</sup> (TO+LA at point *L*). If tentatively assigned as in Fig. 9, which shows a high-resolution (2-cm<sup>-1</sup>) noise-free

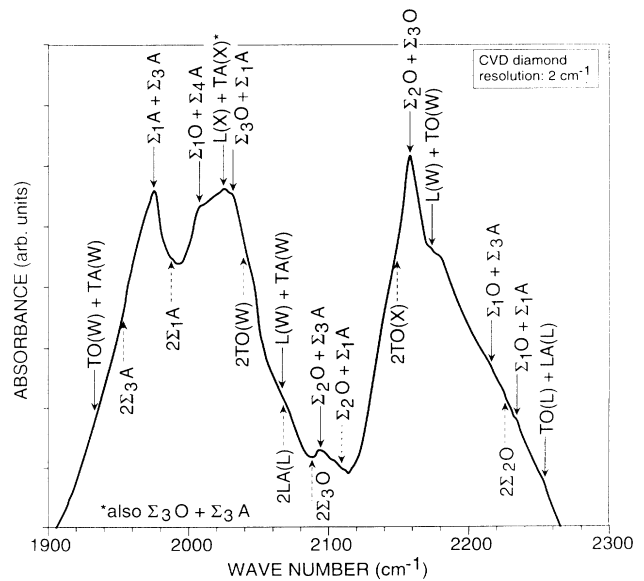


FIG. 9. High-resolution absorbance spectrum of diamond, in the peak two-phonon absorption region (see the caption for Fig. 8).

absorbance trace of diamond in that spectral range, the correlation is seen to be almost perfect. (a) Even the dipole-inactive summations, such as overtones, are in evidence and appear to cause absorption dips. (b) The two sharp peaks at  $1970\text{ cm}^{-1}$  ( $\Sigma_1A + \Sigma_3A$ ) and  $2153\text{ cm}^{-1}$  ( $\Sigma_2O + \Sigma_3O$ ) both involve phonon branches that have accidental critical points near the BZ boundary (see Fig. 1), thus giving rise to unusually flat joint dispersion curves and, hence, strong singularities in the combined density of modes. (c) There is one single feature that cannot be explained in terms of our zone-edge CP's: The poorly resolved doublet at approximately  $2172\text{-}2178\text{ cm}^{-1}$  may relate to an  $L(W) + \text{TO}(W)$  combination but the next nearest summation,  $\Sigma_1O + \Sigma_3A$ , is at  $2217\text{ cm}^{-1}$ , which is much too far.

At this point, we may also wish to assess the validity of our assignments in the light of earlier, independent investigations of the two-phonon absorption process in type-IIa diamond; this is best done as summarized in Table II, which lists the positions, in millielectronvolts, of the 17 spectral features observed by Hardy and Smith<sup>5</sup> and by Wehner *et al.*<sup>11</sup> (a) Our assignments (column 4) yield 15 calculated positions (column 5) that fit the data with an error of less than 0.3% if the CP phonon energies are as listed in Table I. One half of these assignments are technically ir inactive, which emphasizes again (see Fig. 7) the impact of residual impurities, even in IIa-classified material. (b) The assignments proposed by Solin and Ramdas<sup>6</sup> (third column) fail to include six of the 17 features reported in Refs. 5 and 11; still, many of their assignments are in accord with the results of our work. (c) Feature no. 10, which is ascribed to an  $L + \text{TO}$  summation at point  $W$ , in both the third and fourth columns, ac-

tually refers to the  $2172\text{-}$  and  $2178\text{-cm}^{-1}$  doublet discussed earlier and does not fit any of the CP phonon models. The same comment applies to feature no. 13, that is, the sharp turnaround at  $2332\text{ cm}^{-1}$  already considered in conjunction with Fig. 8.

Finally, we may "examine the phonons" in the context of the Raman-Stokes experiments that were carried out by Solin and Ramdas.<sup>6</sup> These experiments shed additional light on the second-order process because overtones are known to be Raman active in most representations, whereas combinations are strongly polarization dependent.<sup>18</sup> The Raman spectrum we found of most value, in the sense of best complementing ir-absorption data, is the one shown in Fig. 10, which refers to a  $Z'(X'Z')Y'$  geometry; this means that incident light propagates in the  $[001]$  crystallographic direction and is polarized along  $[110]$ , but the measured scattered light is along the  $[1\bar{1}0]$  axis and has a  $[001]$  polarization vector. The spectrum consists of a continuous background upon which are superimposed a sequence of slope discontinuities and a broad peak shifted by about  $2460\text{-cm}^{-1}$  wave numbers. The features are essentially temperature independent and, if clearly recognizable, are labeled (see Fig. 10) in accord with the Solin-Ramdas nomenclature. Nine of the 11 discontinuities can be immediately identified as Raman-allowed summations of CP phonons, in the  $\Gamma^{(25+)}$  representation, and five of these assignments (they are underlined in Fig. 10) fit the Solin-Ramdas scheme. The Raman peak at  $2460\text{ cm}^{-1}$  (features no. 7 and 8) cannot be attributed to a single CP phonon summation and does not "show" in transmission (see Fig. 3), which points to dipole-inactive transitions. Pending further investigations, we suggest that the peak emerges as a result of the

TABLE II. Critical-point analysis of diamond two-phonon absorptions.

Spectral feature <sup>a</sup>	Measured position <sup>b</sup> (meV)	Assignment (Ref. 6)	Assignment (this work)	Calculated position (meV)	Brief comment <sup>c</sup>	
1	<i>s</i>	225	$\text{LO}(L) + \text{TA}(L)$	$\text{LO}(L) + \text{TA}(L)$	$224 \pm 1$	
2	<i>k</i>	232	$\text{TO}(X) + \text{TA}(X)$	$\Sigma_2O + \Sigma_4A$	$232 \pm 1$	
3	<i>p</i>	244	$\Sigma_1A + \Sigma_3A$	$\Sigma_1A + \Sigma_3A$	$244 \pm 1$	
4	<i>m</i>	247	$\text{L}(X) + \text{TA}(X)$	$2\Sigma_1A$	$246 \pm 1$	<i>D</i> inactive
5	<i>p</i>	251	$\Sigma_3O + \Sigma_3A$	$\Sigma_3O + \Sigma_3A$	$250 \pm 1$	
6	<i>k</i>	253	$\Sigma_3O + \Sigma_1A$	$2\text{TO}(W)$	$253 \pm 1$	<i>D</i> inactive
7	<i>m</i>	258	$\Sigma_2O + \Sigma_3A$	$2\Sigma_3O$	$258 \pm 1$	<i>D</i> inactive
8	<i>m</i>	262		$\Sigma_2O + \Sigma_1A$	$261 \pm 1$	<i>D</i> inactive
9	<i>p</i>	267	$\Sigma_2O + \Sigma_3O$	$\Sigma_2O + \Sigma_3O$	$267 \pm 1$	
10	<i>s</i>	270	$\text{L}(W) + \text{TO}(W)$	$\text{L}(W) + \text{TO}(W)$	$268 \pm 1$	no fit
11	<i>k</i>	274	$\Sigma_1O + \Sigma_3A$	$\Sigma_1O + \Sigma_3A$	$275 \pm 1$	
12	<i>s</i>	281	$\text{LO}(L) + \text{LA}(L)$	$\text{L}(X) + \text{TO}(X)$	$281 \pm 1$	
13	<i>m</i>	289				no CP assignment
14	<i>k</i>	292		$\Sigma_1O + \Sigma_2O$	$291 \pm 1$	<i>D</i> inactive
15	<i>s</i>	302		$2\text{TO}(L)$	$303 \pm 1$	<i>D</i> inactive
16	<i>s</i>	315		$2\text{LO}(L)$	$311 \pm 1$	<i>D</i> inactive
17	<i>m</i>	330		$2\text{O}(\Gamma)$	$330 \pm 1$	ir inactive

<sup>a</sup>*k*=kink; *m*=minimum; *p*=peak, *s*=shoulder.

<sup>b</sup>As listed in Refs. 5 and 11.

<sup>c</sup>Refers to our assignments (CP=critical point; *D*=dipole; ir=infrared).

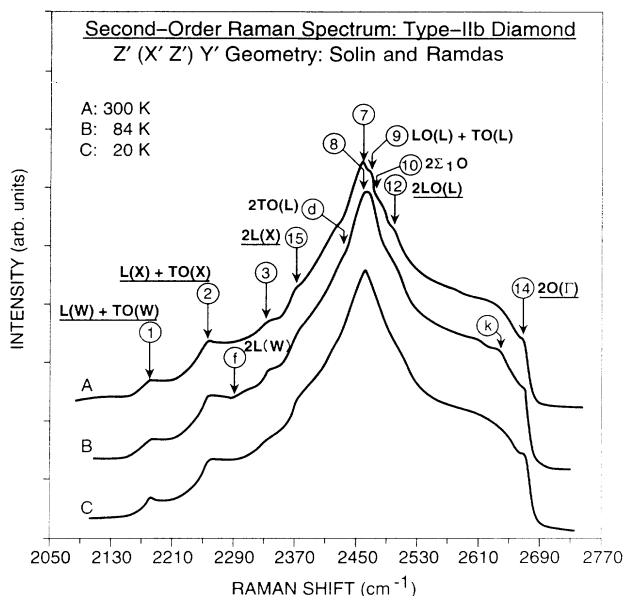


FIG. 10. Second-order optical-phonon Raman-Stokes spectrum of diamond as recorded in Fig. 5 of Ref. 6. Our assignments are based on critical-point phonon frequencies listed in Table I, fifth column. Underscored assignments are in accord with assignments made in Ref. 6.

activation of the overtone at  $2440 \text{ cm}^{-1}$  ( $2\text{TO}$  at point  $L$ ) and the nearby overtone at  $2478 \text{ cm}^{-1}$  ( $2\Sigma_1\text{O}$ ), which combine to produce an apparent joint-density-of-modes singularity at

$$[2\text{TO}(L) + 2\Sigma_1\text{O}]/2 = 2459 \pm 4 \text{ cm}^{-1}, \quad (12)$$

the  $\text{LO}(L) + \text{TO}(L)$  combination then appearing as a shoulder on the high-frequency side of the spectrum. Feature no. 3 at  $2333 \text{ cm}^{-1}$  is also of significance because it obviously corresponds to the ir absorption at  $289 \text{ meV}$  ( $2332 \text{ cm}^{-1}$ ), for which we have no CP related interpretation (see Table II). Interestingly, Solin and Ramdas<sup>6</sup> noticed that "this feature was unique in that its shape is dependent on the type of diamond examined," which would indeed confirm that it is not of an intrinsic nature.

## VI. CONCLUSION

The phonon-dispersion curves obtained by means of inelastic neutron-scattering experiments are not sufficiently accurate to test the available lattice-dynamical models<sup>13</sup> or to yield exact CP phonon frequencies for interpreting the second-order optical spectra of diamond. A comprehensive analysis of such spectra was attempted by Solin and Ramdas<sup>6</sup> but failed to be entirely successful<sup>7</sup>

because it is not a straightforward task to assign second-order infrared absorption or Raman-scatter features to specific two-phonon summations considering the multiplicity of nondegenerate phonon branches. Much remains to be done to properly describe the lattice dynamics of diamond crystals.

Perfect diamond-type lattices are transparent in the first order; in the presence of defects, however, absorption can occur because impurities, imperfections, or disorder disrupt the translational symmetry of the lattice.<sup>3</sup> Defect-activated one-phonon absorptions thus can provide direct information on lattice vibrational modes and can be quite effective for obtaining the CP phonon frequencies and identifying the nature of residual impurities and/or defect centers. Since the CVD diamonds of current interest are polycrystalline and defect rich, we have taken advantage of this situation for locating the CP phonons with much improved accuracy, using the neutron-spectroscopy data for guidance.

The background-subtraction technique discussed in Sec. III yields a surprisingly rich absorption structure at wave numbers below the  $1332.5\text{-cm}^{-1}$  band-mode cutoff (see Figs. 5 and 6). Dipole activity is seen to be generated by nitrogen-associated defect centers, which allows us to detect the 16 zone-edge CP phonons of diamond, in addition to the zone-center Raman mode. Their frequencies are listed in Table I; the sum rule does not hold, but we find that Brout's sum at point  $\Gamma$  is in good agreement with the Mitra-Marshall formula.<sup>32</sup>

This set of CP phonons then provides the basis for predicting the positions of second-order features through simple summations. The procedure yields excellent results for two-phonon ir absorptions (see Figs. 8 and 9) but for the kink at  $2332 \text{ cm}^{-1}$ ; beyond that point, there are no dipole-active summations, which leads to the conclusion that the diffuse absorption of diamond at the high-frequency end of the two-phonon region reflects a relaxation of the selection rules. Regarding earlier investigations of the two-phonon absorption process,<sup>5,11</sup> our assignments (see Table II) predict the positions of 15 out of the 17 observed features with an error of less than 0.3%.

Similar conclusions apply to the second-order Raman spectrum<sup>6</sup> in the sense that nine of the 11 discontinuities recorded in the  $Z'(X'Z')Y'$  polarization geometry can be immediately identified as  $\Gamma^{(25+)}$ -allowed summations; five of these assignments fit the Solin-Ramdas scheme. The broad peak at  $2460 \text{ cm}^{-1}$  cannot be attributed to a single CP summation but may emerge as a result of the simultaneous activation of the  $\text{TO}(L)$  and  $\Sigma_1\text{O}$  overtones. The Raman feature at  $2333 \text{ cm}^{-1}$  is of particular interest because it mirrors the absorption feature at  $2332 \text{ cm}^{-1}$  for which there is no CP-related interpretation, thus pointing to an accidental mode singularity or a nonintrinsic process.

<sup>1</sup>W. A. Yarbrough and R. Messier, *Science* **247**, 688 (1990).

<sup>2</sup>C. A. Klein, *SPIE Crit. Rev.* **38**, 204 (1991).

<sup>3</sup>J. T. Houghton and S. D. Smith, *Infra-Red Physics* (Oxford University Press, London, 1966), Chap. 3.

<sup>4</sup>J. L. Warren, J. L. Yarnell, G. Dolling, and R. A. Cowley, *Phys. Rev.* **158**, 805 (1967).

<sup>5</sup>J. R. Hardy and S. D. Smith, *Philos. Mag.* **6**, 1163 (1961).

<sup>6</sup>S. A. Solin and A. K. Ramdas, *Phys. Rev. B* **1**, 1687 (1970).

- <sup>7</sup>C. D. Clark, E. W. J. Mitchell, and B. J. Parsons, in *The Properties of Diamond*, edited by T. Field (Academic, London, 1979), Chap. 2.
- <sup>8</sup>M. Lax and E. Burstein, *Phys. Rev.* **97**, 39 (1955).
- <sup>9</sup>S. D. Smith and J. R. Hardy, *Philos. Mag.* **5**, 1311 (1960).
- <sup>10</sup>C. Klein, T. Hartnett, R. Miller, and C. Robinson, in *Proceedings of the Second International Symposium on Diamond Materials*, edited by A. Purdes *et al.* (ECS, Pennington, NJ, 1991), p. 435.
- <sup>11</sup>R. Wehner, H. Borik, W. Kress, A. A. Goodwin, and S. D. Smith, *Solid State Commun.* **5**, 307 (1967).
- <sup>12</sup>The reader may find additional dispersion curves, for the  $Z$  direction ( $X \rightarrow W$ ) in particular, on p. 308 of Ref. 11.
- <sup>13</sup>C. Patel, W. F. Sherman, and G. R. Wilkinson, *J. Phys. C* **17**, 6063 (1984).
- <sup>14</sup>R. Tubino, L. Piseri, and G. Zerbi, *J. Chem. Phys.* **56**, 1022 (1972).
- <sup>15</sup>P. G. Dawber and R. J. Elliott, *Proc. Phys. Soc. (London)* **81**, 453 (1963).
- <sup>16</sup>Evidently, the factor  $|X(\omega)|^2$  can generate peaks within the allowed frequency band; their position depends upon the nature of the defect, hence provides a signature of much value for identifying specific impurities in diamond and, thus, for classifying gem-quality diamonds (see Ref. 7).
- <sup>17</sup>Note that certain summations of phonon branches lead to particularly flat joint dispersions, which results in abnormally high densities of modes and translates into sharp peaks, at some frequencies.
- <sup>18</sup>J. L. Birman, *Theory of Crystal Space Groups and Lattice Dynamics* (Springer-Verlag, Berlin, 1984), Chap. N.
- <sup>19</sup>D. S. Knight and W. B. White, *J. Mater. Res.* **4**, 385 (1989).
- <sup>20</sup>J. W. Ager, D. K. Veirs, and G. M. Rosenblatt, *Phys. Rev. B* **43**, 6491 (1991).
- <sup>21</sup>K. C. Hass, M. A. Tamor, T. R. Anthony, and W. F. Banholzer, *Phys. Rev. B* **44**, 12046 (1991).
- <sup>22</sup>D. F. Edwards and H. R. Philipp, in *Handbook of Optical Constants of Solids*, edited by E. Palik (Academic, Orlando, 1985), p. 665.
- <sup>23</sup>X. X. Bi, P. O. Eklund, J. G. Zhang, A. M. Rao, T. A. Perry, and C. P. Beetz, *J. Mater. Res.* **5**, 811 (1990).
- <sup>24</sup>C. Wild, N. Herres, J. Wagner, P. Koidl, and T. R. Anthony, in *Proceedings of the First International Symposium on Diamond and Diamond-Like Films*, edited by J. Dismukes *et al.* (ECS, Pennington, NJ, 1989), p. 283.
- <sup>25</sup>In the wave-number range of interest here, the absorbance of this specimen almost mirrors the frequency dependence of the calculated density of modes (Ref. 14), especially the strong and broad peak associated with optical-phonon branches. This may not be particularly meaningful, considering how the baseline fitting was implemented, but it provided the impetus to search for additional CP's and clearly established that defect-activated lattice vibrational modes dominate the absorption in the one-phonon region. See also Fig. 5 of Ref. 10.
- <sup>26</sup>G. Davies, *Chem. Phys. Carbon* **13**, 2 (1977).
- <sup>27</sup>In the wave-number range around  $1000 \text{ cm}^{-1}$ , these uncertainties are comparable to the differences between CP phonon frequencies, particularly with respect to the  $\Sigma$ -direction branches (see Fig. 1).
- <sup>28</sup>L. H. Robins, L. P. Cook, E. N. Farabaugh, and A. Feldman, *Phys. Rev. B* **39**, 13367 (1989).
- <sup>29</sup>D. W. Feldman, J. H. Parker, W. J. Choyke, and L. Patrick, *Phys. Rev.* **173**, 787 (1968).
- <sup>30</sup>Note that two permutations [ $LA(L)/\Sigma_3O$  and  $\Sigma_1A/TO(W)$ ] were executed to update the CP phonon tabulation published earlier (Ref. 10).
- <sup>31</sup>H. B. Rosenstock and G. Blanken, *Phys. Rev.* **145**, 546 (1966).
- <sup>32</sup>S. S. Mitra and R. Marshall, *J. Chem. Phys.* **41**, 3158 (1964).
- <sup>33</sup>J. E. Field, in *The Properties of Diamond*, edited by J. Field (Academic, London, 1979), Chap. 21.
- <sup>34</sup>We note, however, that while the  $O(\Gamma)$  line appears to be very weak, a strong absorption band emerges at  $1310 \text{ cm}^{-1}$ , which points to an ir-active vibrational mode of the 21R diamond polytype [K. E. Spear, A. W. Phelps, and W. B. White, *J. Mater. Res.* **5**, 2277 (1990)]. Similarly, the doublet we observe at 662 and  $669 \text{ cm}^{-1}$  in CVD diamond (see Fig. 6) may well signal an ir-active mode of the postulated 8H diamond structure. These assignments are obviously rather tentative and will require confirmation by other means.
- <sup>35</sup>M. E. Thomas and R. I. Joseph, *SPIE Proc.* **1326**, 120 (1990).
- <sup>36</sup>Difference bands have essentially zero intensity when  $\hbar\omega_1$  and  $\hbar\omega_2$  are both much larger than  $k_B T$ , as is the case for diamond at room temperature (see Ref. 3).